PERFORMANCE OF POROUS MARINE STRUCTURES OF SINGLE AND DOUBLE PERFORATED SEAWALLS IN REGULAR OBLIQUE WAVES

Nadji Chioukh[1,2], Mohamed Boukhari[2], Yalçın Yüksel[3], Benameur Hamoudi[2]

In the present paper we examine the performance of two very common types of wave absorbing porous marine structures under regular oblique waves. The first structure consists of a single perforated vertical seawall, whereas the second consists of two perforated vertical seawalls creating what is called a chamber system (Jarlan type breakwater). The structures are surface piercing thus eliminating wave overtopping. Two methods are used for the present investigation. In the first method the problem of the interaction of obliquely incident linear waves upon a pair of porous vertical seawalls is first formulated in the context of the linear diffraction theory. The resulting boundary integral equation, which is matched with far-field solutions represented in terms of analytical series with unknown coefficients, and appropriate boundary conditions at the free surface, seabed and seawalls, is then solved numerically using the multi-domain boundary element method. In the second method a semi-analytical solution is developed by means of the eigenfunction expansions and a minimization approach using a least square method. In both methods the dissipation of the wave energy due to the presence of the perforated seawalls is represented by a simple yet effective relation in terms of the porosity parameter appropriate for thin perforated walls. The results are presented in terms of reflection and transmission coefficients, and the wave energy dissipation. Effects of the incident wave angles, porosities and depths of the walls and other major parameters of interest are explored.

Keywords: oblique regular waves; perforated seawalls; boundary element; eigenfunction expansions; reflection coefficient; transmission coefficient

INTRODUCTION

In coastal areas it has been found efficient to use breakwaters to prevent the passage of incident waves and currents. The primary function of these coastal structures is to reduce wave transmission to protect shores and create calmer areas such as in ports and marinas, for safer operations of maritime transport. In some cases it has been found customary to use perforated vertical seawalls as breakwaters. The porosity provided by the perforations enhances wave dissipation, and hence reduces wave reflection and transmission. In the mean time exchange of waters between both the sea and the shore sides of the walls is not totally inhibited. Perforations of the seawalls are usually made by leaving out square or circular openings in the walls.

For the past three decades there has been tremendous research (experimental and theoretical) dedicated to the study of seawall breakwaters for perpendicular wave incidences. A good review is given by Huang et al. (2011). Most of these works were carried out to achieve a reduction in wave reflections and transmissions primarily, and structure stability at the same time. Numerical methods have helped in the validation work and the setting of simple analytical methods for quick evaluations. These numerical methods are now well established and are used with confidence to analyse a variety of breakwater configurations.

Whereas seawall breakwaters have been extensively investigated for perpendicular wave attacks, oblique waves have been considered less due to the occurrence of some important experimental shortcomings. In wave flumes it is almost impossible to investigate oblique waves due to the reflections that arise from the side walls. Unless the waves are damped on the flume sides to prevent the occurrence of these added reflections, one cannot carry out such investigations. However, there exist quite a number of good references relating to theoretical works for investigating the interaction of oblique waves and seawalls, see for example Das et al. (1997), Porter (1995), and Liu and Li (2011).

In this paper we present two methods for analysing single and double perforated seawalls. The first is a numerical solution based on the multi-domain boundary element method, and the second is an analytical solution based on the eigenfunction expansions. Analysis is carried out for both single and double perforated seawalls.

THEORETICAL FORMULATIONS

The idealised geometry of the three-dimensional problem is shown in Fig. 1. Regular waves, of small amplitude a, period T and wavelength Li, impinge from the left at an angle α with respect of the

[1] Department of Civil Engineering, University of Djillali Liabes, B.P. No 89, Sidi Bel-Abbes 22000, Algeria
[2] Department of Maritime Engineering, University of Science and Technology MB, B.P. No 1505, Oran 31000, Algeria
[3] Department of Civil Engineering, Yildiz Technical University, Davutpaşa Caddesi, 34220 Esenler- İstanbul, Turkey

direction of the axis *x*, in water of depth *d*. Assuming an irrotational flow and incompressible fluid motion, the problem is formulated using a velocity potential $\Phi(x, y, z, t) = \mathrm{Re}[\phi(x, y).e^{\mathrm{i}(k_z z-\omega t)}]$, where Re denotes the real part, $\phi(x, y)$ is the time independent spatial velocity potential, $\mathrm{i} = \sqrt{-1}, \omega = 2\pi / T$ is the wave angular frequency, *t* is the time, and k_z is the *z* component of the wave number $k = 2\pi/Li$. *k* is the solution to the dispersion relation $gk.\tanh(kd) = \omega^2$. The *x* and *z* components of *k* are presented in terms of the angle of incidence α as $k_x = k.\cos\alpha$ and $k_z = k.\sin\alpha$. The wave field is totally specified if $\phi(x, y)$ is known.

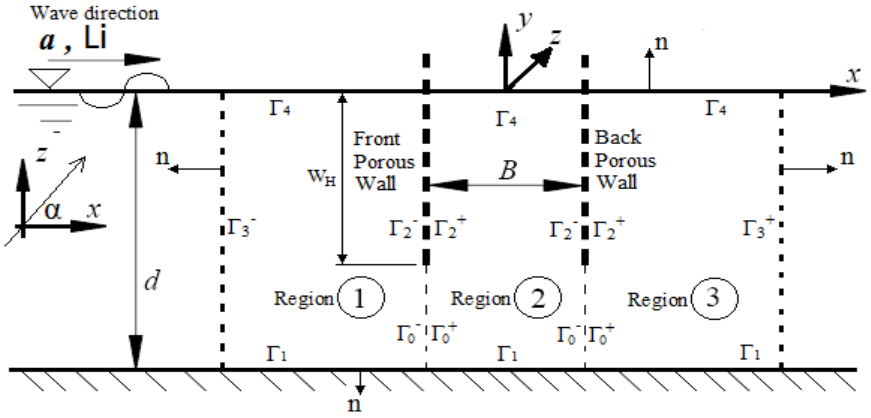

Figure 1. Problem definitions for a breakwater system of double porous walls of height W_H.

We consider a pair of porous walls of height W_H separated by a distance *B* (width of the absorbing chamber) and extending from above the water surface to a certain distance above the channel floor. With this disposition the total fluid domain is divided in three regions as shown in Fig. 1. With sufficient porosity of the walls the waves are transmitted from Region 1 o region 3. The flow in each region could be described by a velocity potential, because of the assumptions of the linear wave theory. Special matching conditions at the interfaces of the flow regions would ensure a smooth transfer of the mass flow from one region to the next. It is worth stating at this stage that in this study the perforated walls are treated as solid homogeneous porous materials.

The spatial velocity potential in each region (*j*) satisfies the following boundary conditions:

$$\frac{\partial^2\phi^{(j)}}{\partial x^2} + \frac{\partial^2\phi^{(j)}}{\partial y^2} - k_z^2.\phi^{(j)} = 0 \quad \text{in fluid region } j = 1, 2, 3 \tag{1}$$

$$\frac{\partial\phi^{(j)}}{\partial n} - \frac{\omega^2}{g}.\phi^{(j)} = 0 \quad \text{for } j = 1, 2, 3 \text{ and } y = 0 \text{ (free surface boundary } \Gamma_4) \tag{2}$$

$$\frac{\partial\phi^{(j)}}{\partial n} = 0 \quad \text{for } j = 1, 2, 3 \text{ and } y = -d \quad \text{(seabed boundary } \Gamma_1) \tag{3}$$

$$\left.\begin{aligned} &\frac{\partial\left(\phi^{(1)} - \phi_I\right)}{\partial n} - \mathrm{i}.k_x.\left(\phi^{(1)} - \phi_I\right) = 0 \quad \text{(radiation condition at } x \to -\infty) \\ &\frac{\partial\left(\phi^{(3)}\right)}{\partial n} - \mathrm{i}.k_x.\left(\phi^{(3)}\right) = 0 \quad \text{(radiation condition at } x \to +\infty) \end{aligned}\right\} \tag{4}$$

where *g* is the gravitational acceleration, *n* is the normal to the boundary pointing out of a flow region, and ϕ_I is the incident velocity potential.

Moreover, at the interfaces of the flow regions (1) and (2), and (2) and (3), special matching conditions are imposed. Along the fictitious boundaries Γ_0^- and Γ_0^+, continuity requires that:

$$\left.\begin{array}{ll} \phi^{(1)} = \phi^{(2)} \text{ and } \dfrac{\partial \phi^{(1)}}{\partial n} = -\dfrac{\partial \phi^{(2)}}{\partial n} & \text{for } x = -B/2 \text{ and } -d \le y \le -W_H \\ \phi^{(2)} = \phi^{(3)} \text{ and } \dfrac{\partial \phi^{(2)}}{\partial n} = -\dfrac{\partial \phi^{(3)}}{\partial n} & \text{for } x = +B/2 \text{ and } -d \le y \le -W_H \end{array}\right\} \quad (5)$$

For the porous walls (boundaries Γ_2^- and Γ_2^+ respectively relating to the front and back sides of each porous wall), the boundary condition for slotted/perforated walls of Yu (1995) is imposed:

$$\left.\begin{array}{ll} \dfrac{\partial \phi^{(1)}}{\partial n} = -\dfrac{\partial \phi^{(2)}}{\partial n} = \mathrm{i}k.G_1.(\phi^{(1)} - \phi^{(2)}) & \text{for } x = -B/2 \text{ and } -W_H \le y \le 0 \\ \dfrac{\partial \phi^{(2)}}{\partial n} = -\dfrac{\partial \phi^{(3)}}{\partial n} = \mathrm{i}k.G_2.(\phi^{(2)} - \phi^{(3)}) & \text{for } x = +B/2 \text{ and } -W_H \le y \le 0 \end{array}\right\} \quad (6)$$

G is a dimensionless complex quantity. The subscripts 1 and 2 refer respectively to the front and back wall. This quantity is known as the porous effect parameter and can be evaluated by different methods, see Huang (2011). The method of Yu (1995) due to its simplicity is adopted in this study:

$$G = \frac{P}{k.\delta.(f - \mathrm{i}.s)} = |G|.e^{\mathrm{i}.\theta} \quad \text{for } 0 \le \theta \le \pi/2 \quad (7)$$

where δ is the thickness of the wall, f is the linearized resistance coefficient, $s = 1 + Cm(1\text{-}P)/P$ is an inertia coefficient, and θ is the argument of the complex part of *G*. For thin porous walls the argument θ, which is associated with the added mass (*Cm*), is usually not significant and can be treated as zero ($\theta \approx 0$ and $Cm \approx 0$), and hence it is customary to use s=1. The linearized resistance coefficient f is estimated from the empirical relation of Li et al. (2006), $f = -3338.7(\delta/d)^2 + 82.769(\delta/d) + 8.711$, which is valid in the range $0.0094 \le \delta/d \le 0.05$.

Numerical solution by the multi-domain boundary element method (MDBEM)

To solve the problem, the radiation condition of Eq. (4) is treated by truncating regions (1) and (3) at two fictitious vertical boundaries respectively at distances $x = -l$ (boundary Γ_3^-) and $x = +l$ (boundary Γ_3^+). The velocity potentials at these boundaries are represented in terms simple relations with unknown coefficients to be solved as part of the numerical method:

$$\left.\begin{array}{l} \phi^{(1)} = \left(e^{\mathrm{i}k_x.(x+l)} + R_0.\mathrm{e}^{-\mathrm{i}k_x(x+l)}\right) I_0(\mathrm{y}) \quad \text{and} \quad \dfrac{\partial \phi^{(1)}}{\partial n} = -\dfrac{\partial \phi^{(1)}}{\partial x} \quad \text{for } x = -l \quad (\text{boundary } \Gamma_3^-) \\ \phi^{(3)} = \left(T_0.e^{\mathrm{i}k_x(x-l)}\right) I_0(y) \quad \text{and} \quad \dfrac{\partial \phi^{(3)}}{\partial n} = \dfrac{\partial \phi^{(3)}}{\partial x} \quad \text{for } x = +l \quad (\text{boundary } \Gamma_3^+) \end{array}\right\} \quad (8)$$

where $I_0(y) = -\dfrac{a.Li}{T}.\dfrac{\cosh[k.(y+d)]}{\sinh(k.d)}$, and R_0 and T_0 are unknown complex coefficients to be determined.

The physical problem described by Eqs. (1), (2), (3), (5), (6), and (8), is transformed to integral equations using the Green's theorem, and then solved by a MDBEM. Further details of the method can be found in Koley et al. (2015a, 2015b). For smooth (constant) elements the general form of the integral equation is written as:

$$\frac{1}{2}\phi_i^j(x,y) + \int_{\Gamma^j}\left(\frac{\partial Q}{\partial n}\phi^j(x',y') - Q\frac{\partial \phi^j(x',y')}{\partial n}\right).\mathrm{d}\Gamma = 0 \quad (\text{for region } j = 1,2,3) \quad (9)$$

This equation relates the potentials ϕ_i^j of the source points, $P(x,y)$, to ϕ^j and its normal derivative $\partial\phi^j/\partial n$ of the field points, $P'(x',y')$, lying on a boundary Γ^j of a flow region (j=1,2,3). For region (1) the boundary $\Gamma^1 = \Gamma_1 + \Gamma_0^- + \Gamma_2^- + \Gamma_4 + \Gamma_3^-$, for region (2) the boundary

$\Gamma^2 = \Gamma_1 + \Gamma_0^- + \Gamma_2^- + \Gamma_4 + \Gamma_2^+ + \Gamma_0^+$, and for region (3) the boundary $\Gamma^3 = \Gamma_1 + \Gamma_3^+ + \Gamma_4 + \Gamma_2^+ + \Gamma_0^+$ (see Fig. 1). Q is the free space fundamental solution of the Modified Helmholtz equation. It depends only on the distance $r = \sqrt{(x-x')^2 + (y-y')^2}$, and is given together with its normal derivative as:

$$Q = -\frac{1}{2\pi} K_0(k_z.r) \quad \text{and} \quad \frac{\partial Q}{\partial n} = \frac{\partial Q}{\partial r}.\frac{\partial r}{\partial n} = \frac{k_z}{2\pi} K_1(k_z.r).\frac{\partial r}{\partial n} \tag{10}$$

K_0 and K_1 are respectively the zeroth and the first order of the modified Bessel functions of the second kind. The quantity $(\partial r / \partial n)$ defines the direction cosines of the normal to an element. When $r \to 0$ K_0 has an asymptotic behaviour and is approximated as $K_0(k_z.r) = -0.5772 - \ln(k_z.r/2)$.

Eq. (9) is applied consecutively to all source points in each fluid region (j). For the numerical implementation of the MDBEM the total boundary Γ^j of each region is discretised into a number of N^j elements (N^1, N^2, N^3 correspond to the number of elements-nodes respectively for region 1, 2, and 3). Variations of the variables over the elements are assumed to be constant and the unknowns are defined at the mid-elements nodes. The resulting discretised integral equations are written in the following general discrete forms:

$$\sum_{i=1}^{N^j}\sum_{m=1}^{N^j}\left[\int_{\Delta\Gamma_m}\left(\frac{\partial Q}{\partial n}.+\frac{\delta_{im}}{2}\right).\mathrm{d}\Gamma\right].\phi_m^j = \sum_{i=1}^{N^j}\sum_{m=1}^{N^j}\left[\int_{\Delta\Gamma_m} Q.\mathrm{d}\Gamma\right].\frac{\partial \phi_m^j}{\partial n} \qquad (\text{for } j=1,2,3) \tag{11}$$

in which $\Delta\Gamma_m$ is the length of an element (m) part of the boundary Γ^j, and δ_{im} is the Kronecker delta. The discretised form for a region (j) can be rewritten in a matrix form as:

$$\left[\overline{\mathrm{H}}_{im}{}^{(j)}\right]_{N^j \mathrm{x} N^j}.\left\{\phi_m^j\right\}_{N^j} = \left[\overline{\mathrm{G}}_{im}{}^{(j)}\right]_{N^j \mathrm{x} N^j}.\left\{\frac{\partial \phi_m^j}{\partial n}\right\}_{N^j} \qquad (j=1,2,3) \tag{12}$$

$\overline{\mathrm{H}}_{im}{}^{(j)}$ and $\overline{\mathrm{G}}_{im}{}^{(j)}$ are complex coefficients involving integrals of the fundamental solution and its normal derivative along the elements of each flow region (j=1, 2, 3), e.g.:

$$\overline{\mathrm{H}}_{im} = \frac{\delta_{im}}{2} + \int_{\Delta\Gamma_m}\left(\frac{\partial Q}{\partial n}\right).\mathrm{d}\Gamma \qquad \text{and} \qquad \overline{\mathrm{G}}_{im} = \int_{\Delta\Gamma_m} Q.\mathrm{d}\Gamma \Bigg\} \tag{13}$$

These coefficients relate a source point (i) to a field point (m) belonging to an element $\Delta\Gamma_\mathrm{m}$. The integrals in Eq. (13) are evaluated using Gaussian quadrature rules. The discretised system of Eq. (12) is further expanded to include all flow regions (j=1, 2, 3) in one system:

$$\begin{bmatrix} \left[\overline{\mathrm{H}}^{(1)}\right] & 0 & 0 \\ 0 & \left[\overline{\mathrm{H}}^{(2)}\right] & 0 \\ 0 & 0 & \left[\overline{\mathrm{H}}^{(3)}\right] \end{bmatrix}_{N \mathrm{x} N} . \begin{Bmatrix} \left\{\phi^{(1)}\right\} \\ \left\{\phi^{(2)}\right\} \\ \left\{\phi^{(3)}\right\} \end{Bmatrix}_N = \begin{bmatrix} \left[\overline{\mathrm{G}}^{(1)}\right] & 0 & 0 \\ 0 & \left[\overline{\mathrm{G}}^{(2)}\right] & 0 \\ 0 & 0 & \left[\overline{\mathrm{G}}^{(3)}\right] \end{bmatrix}_{N \mathrm{x} N} . \begin{Bmatrix} \left\{\frac{\partial \phi^{(1)}}{\partial n}\right\} \\ \left\{\frac{\partial \phi^{(2)}}{\partial n}\right\} \\ \left\{\frac{\partial \phi^{(3)}}{\partial n}\right\} \end{Bmatrix}_N \tag{14}$$

where N is the total number of constant elements from all flow regions, e.g. $N = N^1 + N^2 + N^3$.

Finally the boundary conditions, expressed by Eqs. (2), (3), (5), (6) and (8), are introduced into Eq. (14). The resulting algebraic system of equations is further rearranged such that all unknowns are moved to one side. It is then solved numerically using a Gaussian elimination algorithm to yield the vector of unknowns (diffracted velocity potentials ϕ (or $\partial\phi/\partial n$) and the coefficients R_0 and T_0). The reflection and transmission coefficients are determined from the following expressions:

$$Cr = |R_0| \quad \text{and} \quad Ct = |T_0| \tag{15}$$

The wave energy loss coefficient Cd, describing the portion of the incident wave energy dissipated by the porous walls, is given by:

$$Cd = 1 - (Cr)^2 - (Ct)^2 \tag{16}$$

Analytical solution by the eigenfunction expansion method

Using the eigenfunction expansion method, the velocity potential in each flow region is expanded in terms of appropriate eigenfunctions. By the separation of variables, the spatial velocity potentials in each flow region j=1, 2, 3 satisfying Eq. (1) along with Eqs (2), (3) and (4) are expressed as:

$$\phi^{(1)} = e^{-n_0.(x+B/2)}.I_0(y) + \sum_{K=0}^{\infty} R_K . e^{n_K(x+B/2)}.I_K(y) \tag{17}$$

$$\phi^{(2)} = \sum_{K=0}^{\infty} A_K . e^{-n_K(x+B/2)}.I_K(y) + \sum_{K=0}^{\infty} B_K . e^{n_K(x-B/2)}.I_K(y) \tag{18}$$

$$\phi^{(3)} = \sum_{K=0}^{\infty} T_K . e^{-n_K(x-B/2)}.I_K(y) \tag{19}$$

where R_K, T_K, A_K and B_K $(K \geq 0)$ are unknown complex coefficients to be determined. The depth dependent eigenfunctions $I_K(y)$ $(K \geq 0)$ are defined as:

$$\left.\begin{aligned} I_0(y) &= -\frac{a.Li}{T}.\frac{\cosh[k.(y+d)]}{\sinh(k.d)} \qquad \text{for } K = 0 \\ I_K(y) &= -\frac{a.Li}{T}.\frac{\cos[m_K.(y+d)]}{\cos(m_K.d)} \qquad \text{for } K = 1, 2, \ldots\ldots \end{aligned}\right\} \tag{20}$$

The eigenvalues m_K's $(K \geq 1)$ are the positive real roots of the dispersion relations $g.m_K.\tan(m_K.d) = -\omega^2$. The values of the n_K's $(K \geq 1)$ are such that $n_K = \sqrt{m_K^2 + k_z^2}$, and $n_0 = -\mathrm{i}.k$.

In the solution procedure the four sets of unknowns are obtained by the matching conditions which are written for convenience as:

$$\frac{\partial \phi^{(1)}}{\partial x} = \frac{\partial \phi^{(2)}}{\partial x} \qquad \text{for } x = -B/2 \text{ and } -d \leq y \leq 0 \tag{21}$$

$$\frac{\partial \phi^{(2)}}{\partial x} = \frac{\partial \phi^{(3)}}{\partial x} \qquad \text{for } x = +B/2 \text{ and } -d \leq y \leq 0 \tag{22}$$

$$\frac{\partial \phi^{(2)}}{\partial x} = \mathrm{i}.k.G_1.(\phi^{(1)} - \phi^{(2)}) \qquad \text{for } x = -B/2 \text{ and } -W_H \leq y \leq 0 \tag{23a}$$

$$\phi^{(1)} = \phi^{(2)} \qquad \text{for x} = -\mathrm{B}/2 \text{ and } -\mathrm{d} \leq \mathrm{y} \leq -\mathrm{W_H} \tag{23b}$$

$$\frac{\partial \phi^{(3)}}{\partial x} = \mathrm{i}.k.G_2.(\phi^{(2)} - \phi^{(3)}) \qquad \text{for } x = +B/2 \text{ and } -W_H \leq y \leq 0 \tag{24a}$$

$$\phi^{(2)} = \phi^{(3)} \qquad \text{for } x = +B/2 \text{ and } -d \leq y \leq -W_H \tag{24b}$$

Following the works of Liu and Li (2011) and Liu et al. (2015), the analytical expressions of the velocity potentials represented by Eqs. (17)-(19) are inserted into Eqs. (21) and (22), and using the orthogonal relation $\int_{-d}^{0} I_J(y).I_K(y).\mathrm{d}z = 0$ $(J \neq K)$ gives:

$$R_K = \delta_{K0} - A_K + e^{-n_K.B}.B_K \tag{25}$$

$$T_K = e^{-n_K.B}.A_K - B_K \tag{26}$$

where $\delta_{KJ}=1$ for $K=J$ and $\delta_{KJ}=0$ for $K\neq J$. Now, inserting Eqs. (17)-(20) and Eqs. (25)-(26) into Eqs. (23)-(24) gives two sets of double series with unknown coefficients A_K and B_K. Using the least square method of Darlimple and Martin (1990) and truncating *K* into *N*, the two double series are transformed into two sets of linear equations that are summarized as:

$$\left.\begin{aligned}\left[\mathrm{a}_{JK}\right]_{N\,x\,N}.\left\{A_K^*\right\}_N+\left[\mathrm{b}_{JK}\right]_{\mathrm{N\,x\,N}}.\left\{B_K^*\right\}_N&=-\left\{\mathrm{c}_I\right\}_N\\ \left[\mathrm{d}_{JK}\right]_{N\,x\,N}.\left\{A_K^*\right\}_N+\left[\mathrm{e}_{JK}\right]_{N\,x\,N}.\left\{B_K^*\right\}_N&=0\end{aligned}\right\} \tag{27}$$

the superscript asterisk (*) denotes the complex conjugate, and the coefficients a, b, c, d, and e are defined as:

$$\mathrm{a}_{JK}=(-2\mathrm{i}kG_1+n_J)(2\mathrm{i}kG_1^*+n_K^*)\int_{-W_H}^{0}I_J(y).I_K(y).\mathrm{dz}+4\int_{-d}^{-W_H}I_J(y).I_K(y).\mathrm{dz} \tag{28a}$$

$$\mathrm{b}_{JK}=(-2\mathrm{i}kG_1+n_J)(-n_K^*.(e^{-n_K.B})^*)\int_{-W_H}^{0}I_J(y).I_K(y).dz \tag{28b}$$

$$\mathrm{c}_I=(-2\mathrm{i}kG_1+n_J)(-2\mathrm{i}kG_1^*)\int_{-W_H}^{0}I_J(y).I_0(y).\mathrm{dz}-4\int_{-d}^{-W_H}I_J(y).I_0(y).\mathrm{dz} \tag{28c}$$

$$\mathrm{d}_{JK}=(-2\mathrm{i}kG_2+n_J)(-n_K^*.(e^{-n_K.B})^*)\int_{-W_H}^{0}I_J(y).I_K(y).\mathrm{dz} \tag{28d}$$

$$\mathrm{e}_{JK}=(-2\mathrm{i}kG_2+n_J)(2\mathrm{i}kG_2^*+n_K^*)\int_{-W_H}^{0}I_J(y).I_K(y).\mathrm{dz}+4\int_{-d}^{-W_H}I_J(y).I_K(y).\mathrm{dz} \tag{28e}$$

Solving the system of linear equations given by Eq. (27) yields the unknowns A_K^* and B_K^*. Using Eqs. (25) and (26), the coefficients R_K and T_K are obtained, and the reflection and transmission coefficients (respectively *Cr* and *Ct*) are simply determined by the relation of Eq. (15).

It is worth to mention that in both methods investigated in this study, fully extended porous walls are treated simply by setting $W_H=d$. For single porous walls they are solved by setting the porosity of the front wall to be sufficiently large ($G_1=\infty$). This way the front wall vanishes and the structure reduces to a single porous wall of porosity P_2 (or simply *P*) and porous parameter G_2 (or simply *G*). In all subsequent computations a large value of $G_1=\infty$ has been taken as 10^8.

METHODS VALIDATION

Some representative results of the coefficients of reflection (*Cr*) and transmission (*Ct*) from both methods investigated in this study have been first validated against results of a number of limiting test cases existing in the literature. Analytical results of Porter (1995) for a single impermeable wall and Das et al. (1997) for double impermeable walls are used as benchmarks.

In Fig. 2 results of *Cr* and *Ct* of a single impermeable wall ($|G_1|=\infty$, $|G_2|=0$) are shown against the incident wave angles α for $W_H/d=0.5$ and $kd=2.0$. It is clearly shown that results of both methods agree very well with those of Porter (1995).

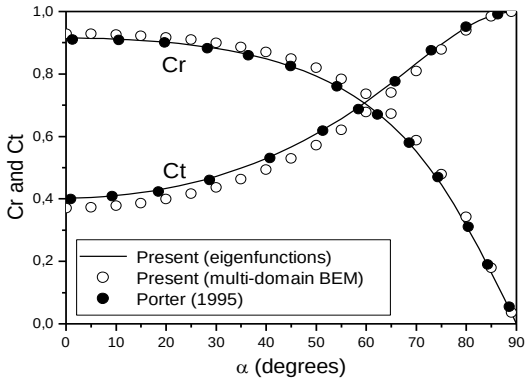

Figure 2. Comparison of *Cr* and *Ct* for a single impermeable wall, $|G_1|=\infty$, $|G_2|=0$, $W_H/d=0.5$, and $kd=2.0$.

In Fig. 3 are shown results of *Cr* for a structure of double impermeable walls ($|G_1|=|G_2|=0$) against values of $\omega^2 d/g$ for an incident wave angle α=30°, W_H/d=0.6, and B/d=2.0. The results of both methods are seen to be in close agreement to those of Das et al. (1997). It is important to mention that results of the present analytical method using the eigenfunction expansions are very similar to those of Liu and Li (2011), who have used the same previous benchmarks to validate their method.

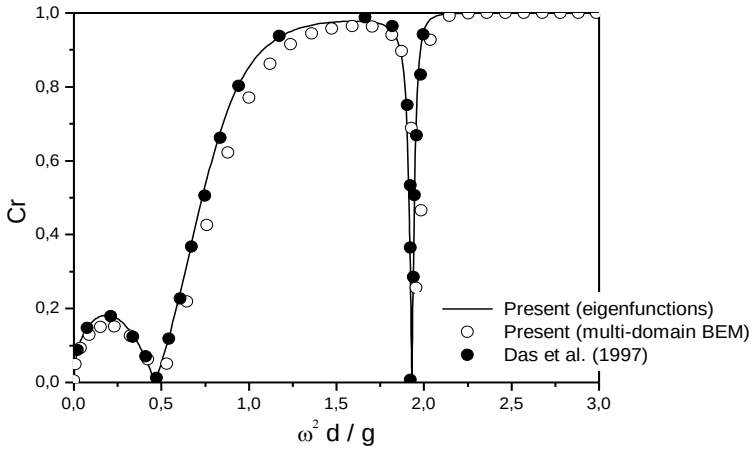

Figure 3. Comparison of *Cr* for double impermeable walls, ($|G_1|=|G_2|=0$), α=30°, W_H/d=0.6, and B/d=2.0.

RESULTS AND DISCUSSION

Due to the large number of parameters in hand, this would lead to too many correlations to investigate. The parameters of interest for correlating the results are the porosities P_1 and P_2 (P for a single porous wall), the relative wall depths W_H/d, the relative water depths kd, the relative chamber widths B/Li, and the wave incidence α. In this work the results are mainly correlated with the incident wave angles.

In Figs. 4-6 are shown effects of the incident wave angles on *Cr* and *Ct* for single porous walls. The numerical results of the BEM method are analogous to the results of the eigenfunction expansions In all of these figures the variations with respect to α show that *Cr* decreases with the increase of α, whereas *Ct* has a reversed trend. These variations fall more rapidly when α>40°. For α=90° all curves of *Cr* and *Ct* tend respectively to 0 and 1.

The variations in Fig. 4 are for different values of W_H/d (0.25, 0.5, and 1.0), and for P=5% and kd=2.5. Irrespective of α *Cr* values increase with increasing W_H/d and *Ct* values decrease. This is logical since extending the wall depth would inhibit the waves from transmitting and hence more reflection would occur. It is also noticed that when W_H/d>0.5 effects of W_H/d become small.

The variations in Fig. 5 are for different values of kd (0.25, 1.5, and 3.5, which correspond respectively to shallow, intermediate, and deep water conditions), and for P=5% and W_H/d=1.0. Irrespective of α *Cr* values increase with increasing kd and *Ct* values decrease. This is sensible since wave reflection is less in shallow water than in deep water. Transmission on the other hand is larger in shallow water than in deep water. Obviously the shallow water waves carry more energy and manage almost all to transmit through the porous wall.

The variations in Fig. 6 are for different values of P (5%, 10%, 20%, and 30%), and for kd=2.5 and W_H/d=1.0. Irrespective of α *Cr* values decrease with increasing P and *Ct* values increase. This is physically understandable since waves would transmit more (and reflect less) when the porous wall has more permeability.

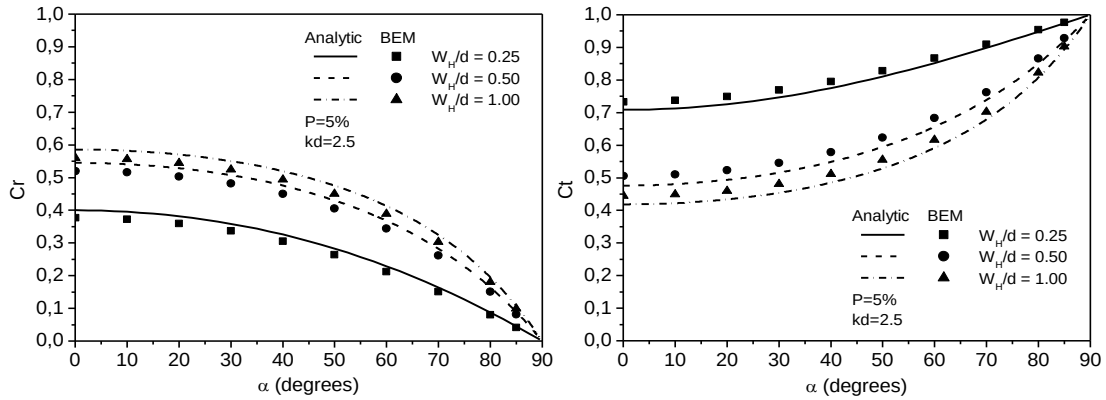

Figure 4. Effects of α on *Cr* and *Ct* for a single porous wall for different values of W_H/d.

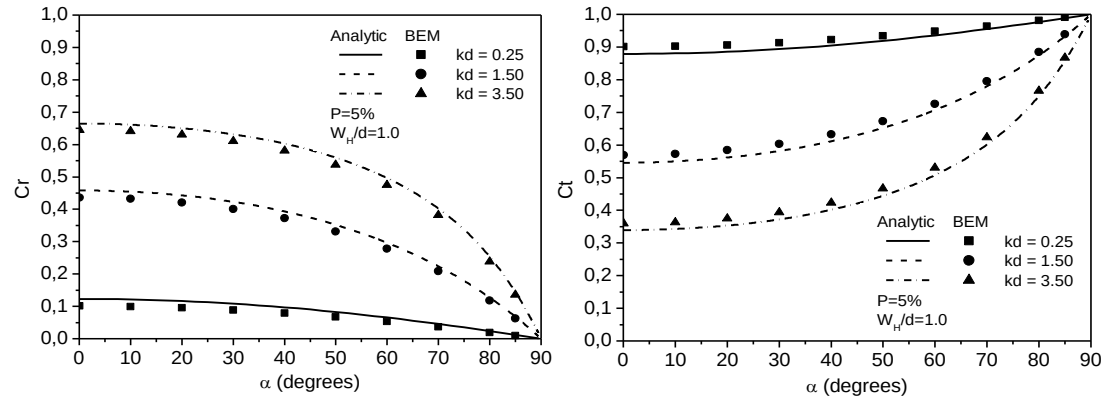

Figure 5. Effects of α on *Cr* and *Ct* for a single porous wall for different values of *kd*.

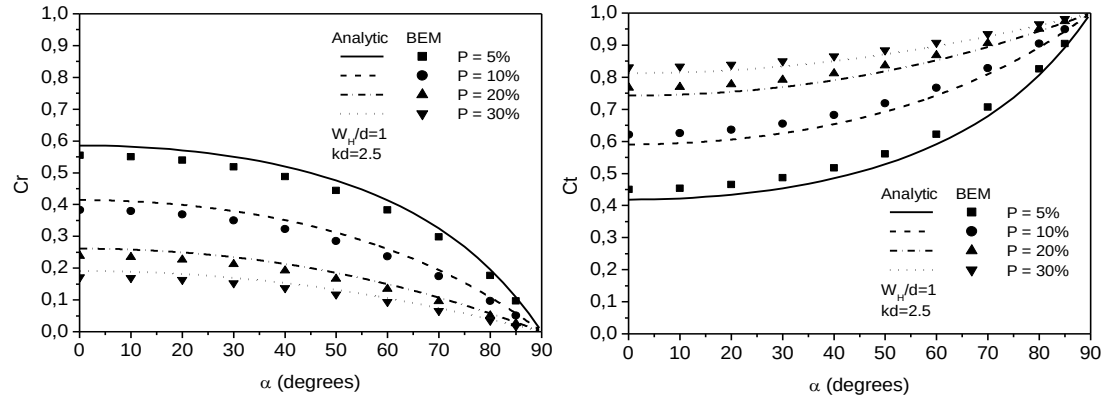

Figure 6. Effects of α on *Cr* and *Ct* for a single porous wall for different values of *P*.

Effects of the incident wave angles on *Cr* and *Ct* for double porous walls are shown in Figs. 7-9. Again the results of both methods developed in the present work are seen to be comparable. In all of these figures the variations with respect to α show that *Cr* presents a depression zone in the middle values of α. *Ct* on the other hand increases in a monotonic fashion exactly as in the case of the single porous wall, with not too much variations for α<40°. Yet again for α=90° *Cr* tends to 0 and *Ct* to 1.

The variations in Fig. 7 are for different values of W_H/d (0.25, 0.5, and 1.0), and for P_1=10%, P_2=5%, *kd*=2.5, and *B/Li*=0.3. Irrespective of α *Cr* values increase with increasing W_H/d and *Ct* values decrease. By adding a second porous barrier the values of *Cr* and *Ct* have decreased compared to the values of the single porous barrier case in Fig. 4.

The variations in Fig. 8 are for different values of *kd* (0.25, 1.5, and 3.5), and for P_1=10%, P_2=5%, W_H/d=1.0, and *B/Li*=0.3. Irrespective of α *Cr* values increase with increasing *kd* and *Ct* values decrease. The values of *Cr* and *Ct* have decreased compared to the values of the single porous barrier case in Fig. 5.

The variations in Fig. 9 are for different values of P_1 (5%, 10%, 20%, and 30%), and for P_2=5%, W_H/d=1.0, *kd*=2.5, and *B/Li*=0.3. Irrespective of α *Cr* values seem to decrease with increasing P_1 and *Ct* values increase. Again the double porous walls breakwater delivers smaller values of *Cr* and *Ct* than those of the single porous barrier case in Fig. 6.

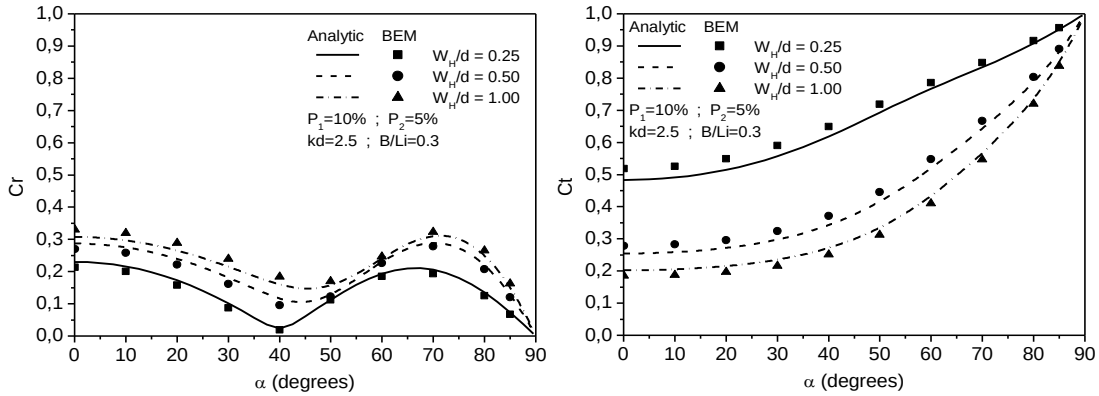

Figure 7. Effects of α on *Cr* and *Ct* for double porous walls for different values of W_H/d.

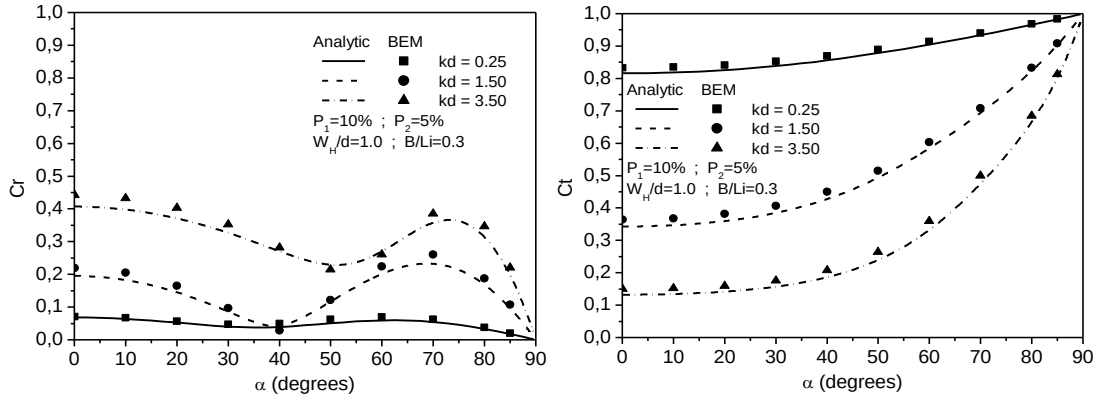

Figure 8. Effects of α on *Cr* and *Ct* for double porous walls for different values of *kd*.

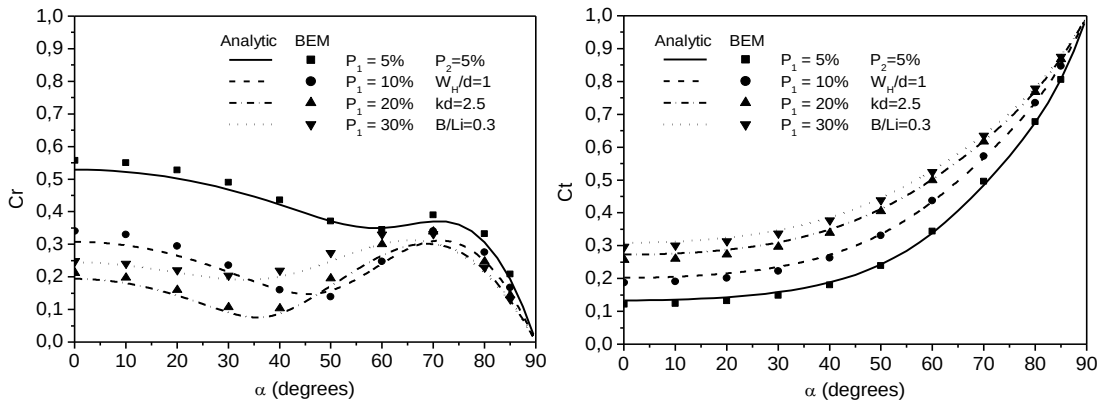

Figure 9. Effects of α on *Cr* and *Ct* for double porous walls for different values of P_1.

In Fig. 10 are shown effects of the relative chamber width *B/Li* on *Cr* and *Ct* for a breakwater of double porous walls for different values of α, and P_1=10%, P_2=5%, W_H/d=1.0, and *kd*=2.5. For normal incident waves (α=0) *Cr* and *Ct* oscillate with minimum values at *B/Li*=0.5*n*+0.25 (*n*=0, 1, 2, …) and maximum values at *B/Li*=0.5*n* (*n*=0, 1, 2, …). The values of *B/Li* corresponding to the minimum and maximum values of *Cr* and *Ct* shift slowly to higher values with the increase of α.

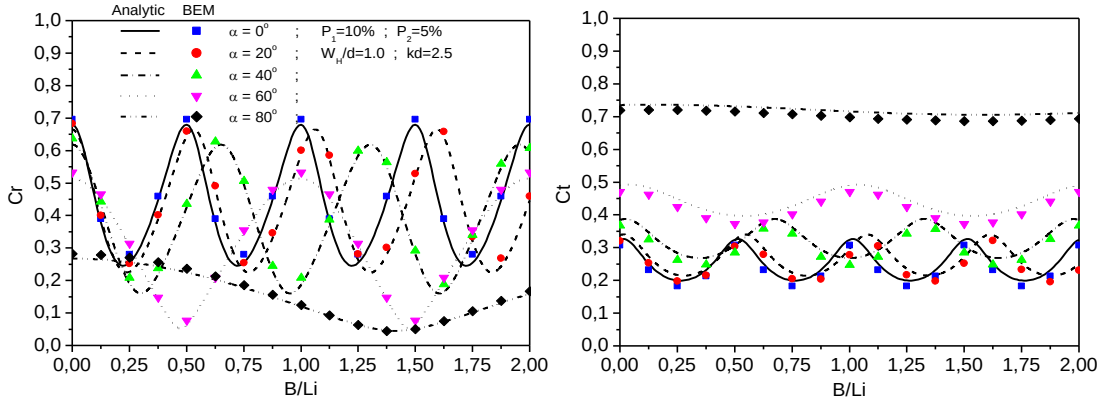

Figure 10. Effects of *B/Li* on *Cr* and *Ct* for double porous walls for different values of α.

CONCLUSIONS

In this work two methods have been developed with the assumptions of potential flow to analyze reflection and transmission of oblique waves from breakwater systems of single and double porous walls. The first is a numerical method based on the multi domain boundary elements, and the second is an analytical method using the eigenfunction expansions. Both methods have been first validated against previous data existing in the literature. In all of the computations of this work the numerical and the analytical results are found to be similar with negligible differences between the two. It has been shown from the present computations that results of coefficients of reflection (*Cr*) and transmission (*Ct*) depend on a large number of parameters. All data of *Cr* and *Ct* have been carefully correlated with these parameters. The correlations revealed meaningful results.

For both breakwater systems of single and double porous walls investigated in this study, the results reveal that the coefficients *Cr and Ct* are not strongly influenced by the incident wave angles for α<40°. Double porous walls breakwaters are shown to deliver smaller coefficients of *Cr and Ct*. Apparently adding a second porous wall to a single porous wall system would create a chamber system

that generates additional wave energy dissipation leading to smaller coefficients of *Cr and Ct*. In practice for normal wave incidence (α=0°), the best distance between the porous walls should be taken as the smallest distance between the walls leading to minimum values of *Cr* and *Ct*, that is *B/Li*=0.25. This value of *B/Li*=0.25 has been found to shift slowly to higher values with the increase of the wave incidence angles α.

REFERENCES

Das, P., Dolai, D., and Mandal, B., 1997. Oblique wave diffraction by parallel thin vertical barriers with gaps. *Journal of Waterway, Port, Coastal, and Ocean Engineering*, ASCE, 123(4), 163–171.

Huang, Z., Li, Y., and Liu, Y., 2011. Hydraulic performance and wave loadings of perforated/slotted coastal structures: A review. *Ocean Engineering*, 38, 1031-1053.

Koley, S., Behera, H., and Sahoo, T., 2015a. Oblique wave trapping by porous structures near a Wall. *Journal of Engineering Mechanics*, ASCE, 141 (3).

Koley, S., Sarkar, A., and Sahoo, T., 2015b. Interaction of gravity waves with bottom-standing submerged structures having perforated outer-layer placed on a sloping bed. *Applied Ocean Research*, 52, 245–260.

Li, Y., Liu, Y., and Teng, B., 2006. Porous effect parameter of thin permeable plates. *Coastal Engineering Journal*, 48(4), 309–336.

Liu, Y., and Li, Y., 2011. The interaction of oblique waves with a partially immersed wave absorbing breakwater. *Proceedings of 32nd International Conference on Coastal Engineering*, ASCE, 32(1).

Liu, Y., Yao, Z. and Li, H., 2015. Analytical and experimental studies on hydrodynamic performance of semi-immersed Jarlan-type perforated breakwaters. *China Ocean Engineering*, 29(6), 793-806.

Porter, R., 1995. Complementary methods and bounds in linear water waves. *Doctoral thesis*, University of Bristol, UK.

Yu, X., 1995. Diffraction of water waves by porous breakwaters. *Journal of Waterway, Port, Coastal, and Ocean Engineering*, ASCE, 121(6), 275–282.